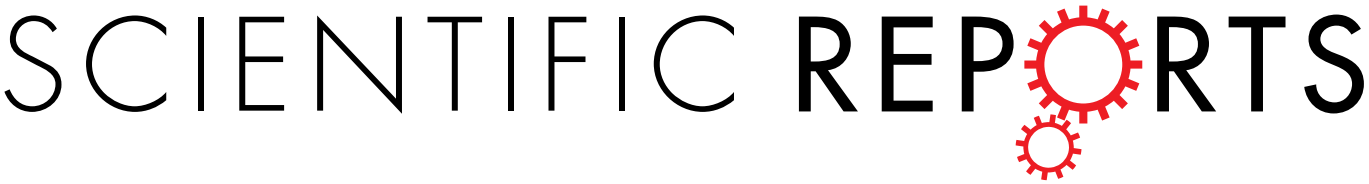

OPEN

Cargo self-assembly rescues affinity of cell-penetrating peptides to lipid membranes

Received: 04 November 2016
Accepted: 16 January 2017
Published: 06 March 2017

Andreas Weinberger[1,*], Vivien Walter[1,*], Sarah R. MacEwan[2,†], Tatiana Schmatko[1], Pierre Muller[1], André P. Schroder[1], Ashutosh Chilkoti[2] & Carlos M. Marques[1]

Although cationic cell-penetrating peptides (CPPs) are able to bind to cell membranes, thus promoting cell internalization by active pathways, attachment of cargo molecules to CPPs invariably reduces their cellular uptake. We show here that CPP binding to lipid bilayers, a simple model of the cell membrane, can be recovered by designing cargo molecules that self-assemble into spherical micelles and increase the local interfacial density of CPP on the surface of the cargo. Experiments performed on model giant unilamellar vesicles under a confocal laser scanning microscope show that a family of thermally responsive elastin-like polypeptides that exhibit temperature-triggered micellization can promote temperature triggered attachment of the micelles to membranes, thus rescuing by self-assembly the cargo-induced loss of the CPP affinity to bio-membranes.

Cationic cell-penetrating peptides (CPPs) such as oligoarginine (Arg_x) or TAT are non-specific enhancers of translocation across the cell membrane. Their efficiency in crossing cell membranes, independent of cell type[1], makes CPPs one of the most valuable tools for cellular delivery of cargo molecules. Although the mechanisms of CPP-assisted translocation are not fully understood, it has been suggested that these short arginine-rich peptides facilitate cellular uptake of their associated cargo by active endocytic pathways independent of membrane receptors[2]. CPPs potentially offer two important advantages over receptor mediated endocytosis for delivery of cargo to cells. First, these cationic oligopeptides do not rely on specific features of cellular physiology, such as heterogeneous receptor expression and are thus applicable to diverse cell types. Second, the action of CPPs can be modulated by a variety of external triggers such as the local arginine concentration, pH and temperature[3].

Interaction with the plasma membrane is the first key step in CPP-assisted translocation. Attractive interactions between CPPs and lipid membranes have been observed for a wide spectrum of simple biomimetic models of the plasma membrane assembled from zwitterionic phopholipids such as DOPC or DOPC/DOPE mixtures, or from mixtures of zwitterionic and anionic phospholipids and cholesterol[4]. Although the affinity of CPPs for membranes appears to hold in a wide range of membrane compositions, membrane permeability to CPPs is only displayed for membranes composed of lipid mixtures with molar fractions of negatively charged lipids that are significantly above typical cell compositions[4,5]. This suggests that translocation across the plasma membrane of cells occurs in a two-stage process, where the CPP first binds to the membrane surface and is then translocated across the cell membrane by endocytosis or other energy-driven pathways. Attachment of cargo molecules to CPPs, however, can perturb this process[3,6,7]. Large macromolecular cargo–peptides, proteins, DNA and polymers–can compromise the attraction of the CPP-cargo to the membrane, either due to size-exclusion or electrostatic effects[1,2,8].

Because the ultimate value of CPPs is to transport cargo across the cell membrane, it is critical to understand the molecular details of the interactions of CPP-cargo constructs with plasma membranes to enable the rational design of intracellular delivery systems using CPPs. We have recently developed a family of stimulus responsive diblock copolymers with blocks composed of elastin-like polypeptides (ELP_{BC}) with a functional CPP head[9]. Here the ELP_{BC} are the cargo attached to the chosen CPP. These amphiphilic ELP_{BC} are an ideal model system to examine molecular details of translocation of CPPs into cells because: 1) they are recombinantly synthesized from a synthetic gene in *Escherichia coli*, so that their sequence and chain length are precisely specified at their

[1]Université de Strasbourg, CNRS, ICS UPR 22, F-67000 Strasbourg, France. [2]Duke University, Department of Biomedical Engineering, Durham, North Carolina, USA. [†]Present address: University of Chicago, Institute for Molecular Engineering, Chicago, Illinois, USA. [*]These authors contributed equally to this work. Correspondence and requests for materials should be addressed to C.M.M. (email: marques@unistra.fr)

ELP construct (hydrophobic/ hydrophilic) pentapeptide block ratios	C-terminal functionality	MW (kDa)	CMT °C	R_h(nm) 25 °C*	R_h(nm) 35 °C*
ELP_{BC} (60/96)	none	61.8	33	6.8 ± 0.1	25.1 ± 0.9
Arg_5-ELP_{BC} (60/96)	Arg_5	62.6	33	6.8 ± 0.2	26.9 ± 0.6
ELP_{BC} (60/60)	none	48.0	34	5.9 ± 0.8	24.0 ± 1.1
Arg_8-ELP_{BC} (60/60)	Arg_8	49.3	31	7.5 ± 0.2	23.5 ± 0.3
TAT-ELP_{BC} (60/60)	TAT	49.6	32	6.0 ± 0.7	25.9 ± 1.4

Table 1. ELP_{BC} and corresponding physical properties in the unimer (25 °C) and micellar state (35 °C). All the samples were also available with an Alexa Fluor 488 fluorophore (AF488) attached to the extremity of the hydrophobic block (N-terminal). The last 3 samples in the table were also prepared with a BODIPY fluorophore instead of AF488. *ELP_{BC} at 20 μM in PBS. Data represents the average of 3 replicates ± standard deviations.

gene level, yielding monodisperse polymers with defined sequence and stereochemistry; 2) different CPPs can be appended to the hydrophilic terminus of the ELP_{BC} at the gene level; 3) these polymers are designed in a diblock architecture with two ELP blocks of different hydrophobicity, and their block composition and length can be tuned to yield ELP_{BC} that undergo micellization at a defined temperature yielding monodisperse micelles with a precisely defined number of polymer chains per micelle[10]. This third feature is of great utility in studying how the cargo architecture controls cell penetration, as self-assembly can be triggered in a relatively narrow temperature range. It allows also to hold constant all other experimental parameters, while morphing the cargo from a unimer polymer chain in a random coil conformation that presents a single CPP moiety at one terminus of the polymer to that of a self-assembled nanoscale object, a spherical micelle that presents multiple copies of the same CPP on its corona. Control of the sequence and chain length of the cargo, the type of CPP and the architecture of the cargo (single unimer polymer chain versus micelle) allows us to examine the effect of cargo properties. We have shown *in vitro* that the self-assembled–micellar state–of ELP_{BC} presenting diverse CPPs can successfully be internalized by several types of cancer cells, while the unassembled state of the ELP_{BC} shows much lower cellular uptake[9,11]. This study revealed that translocation of macromolecular–ELP–cargo is rescued by its self-assembly into micelles. However, the complexity of cells precludes a mechanistic understanding of the process by which translocation of the ELP cargo is rescued by its self-assembly into micelles.

In this paper, we study how self-assembly of ELP_{BC} functionalized with arginine-rich CPPs influences their interaction with Giant Unilamellar Vesicles (GUVs) composed either of the zwitterionic lipid DOPC or of the anionic ternary mixture of DOPC/DOPE/DOPG in molar proportions of 65/25/10. We first investigate interactions and the penetration potential of the CPP-functionalized ELP_{BC} with DOPC GUVs in the unimeric state of the ELP_{BC} and compare these results with observations obtained from incubation of vesicles with ELP_{BC} in their micellar state. We show that attachment of cargo to CPPs reduces the well-known affinity of CPP towards neutral lipid membranes, which can be rescued by cargo self-assembly. Finally, we prove that ELP_{BC} containing a high number of arginine units accumulate in their micellar state on the lipid membrane, but that there is no translocation of the cargo, even in the micellar state, into the GUVs. Results obtained by studying the interactions of ELP_{BC} with the anionic ternary mixture DOPC/DOPE/DOPG, mimicking mammalian cell charge and head lipid content follow the same trend and confirm this picture. By inference, this suggests that micelles that present CPPs on their corona are efficiently taken up by the cell, simply because they accumulate at a high local density at the cell membrane which greatly enhances their uptake by active endocytic mechanisms, rather than by direct penetration. This study also explains the mechanism of how cell penetration of CPPs with attached cargo can be rescued by presenting the CPP at very high local density on a self-assembled nanoparticle, and provides a strategy for the rational design of CPP based intracellular delivery systems.

Results

We used Giant Unilamellar Vesicles (GUVs) composed of DOPC, a zwitterionic lipid, as a model system to investigate lipid-ELP_{BC} interactions. In a typical experiment, the GUVs were incubated in a PBS solution containing 20 μM of ELP_{BC} (See Methods for ELP_{BC} synthesis and Table 1 for physical properties). Interaction behaviour induced by the different CPP functionalities was monitored by confocal microscopy. A small fraction of ELP_{BC}, typically between 0.5–1%, was labeled with a fluorophore attached to the extremity of the hydrophobic block. Since the critical micellization temperature (CMT) for our diblock copolymers is in the range of 31–34 °C, we performed experiments in the unimer state at 25 °C and in the micellar state above the CMT.

The interactions between ELP_{BC} and lipid membranes were monitored by quantitative analysis of fluorescent intensities in the images acquired by confocal fluorescence microscopy. The radial intensity profile of vesicles was recorded at the equatorial plane. An example of normalized intensity profiles for non-interacting (unimer) ELP_{BC} is shown in Fig. 1A. We first discuss changes in affinity due to attachment of cargo to the CPPs and then study the effect of cargo self-assembly on CPP-membrane interactions.

Reduction of affinity due to cargo attachment to CPP sequences. ELP_{BC} functionalized with a CPP sequence can be thought of as macromolecular cargo appended to a cell penetrating functionality. The CPP sequences that we used are known to interact favourably with zwitterionic bilayers. For instance, the protein transduction domain TAT accumulates on membranes of GUVs composed from lipids bearing neutral phosphorylcholine head groups even for bulk concentrations as small as 2 μM[4].

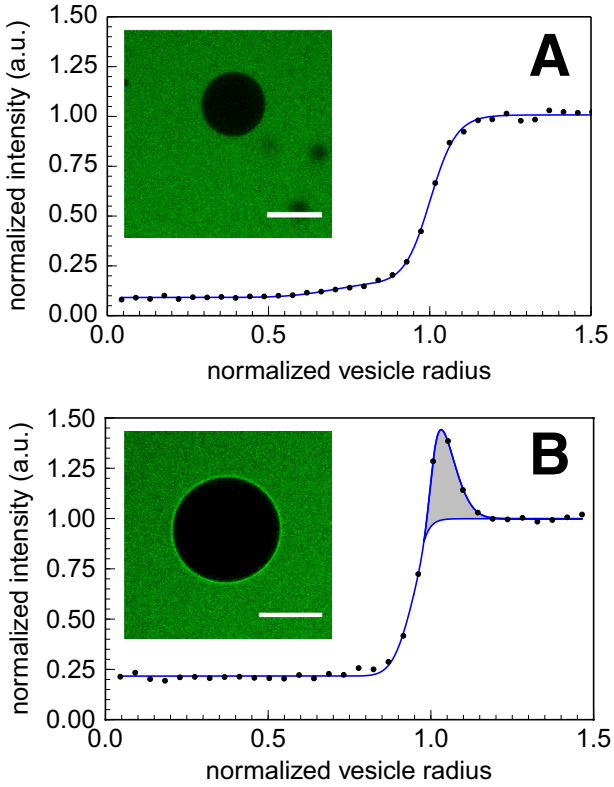

Figure 1. Typical confocal image and intensity radial profiles. Evaluation of the profiles and calculation of the relevant derived quantities are described in the Methods section. (**A**) Radial profile obtained for GUVs dispersed in PBS buffer solution containing functionalized ELP_{BC} unimers at 25 °C. Fluorescence intensity is normalized by the bulk intensity. Vesicle radius (R) is taken at the inflection point of the sigmoidal curve. (**B**) Radial profile across a vesicle after one hour incubation with Arg8- or TAT-functionalized ELP_{BC} in the micellar state above their CMT. The gray area below the peak is proportional to the number per unit surface of ELP_{BC} accumulated on the membrane. Scale bars: 20 μm.

In our experiments, upon incubation of non-functionalized, TAT-, Arg5- or Arg_8-functionalized ELP_{BC} with DOPC-GUVs in the unimer state at 25 °C, we do not observe any accumulation of ELP_{BC} on the membrane, even for concentrations as high as 20 μM, as shown in the top panel of Fig. 1. Attachment of a polymer cargo to the TAT peptide sequence reduces the known affinity[4] of CPPs with respect to the membrane, as expected from fundamental arguments of entropy reduction of polymers near interfaces[12]. Indeed, the number of conformations available for a polymer in the bulk solution is larger than those near an impenetrable wall, leading to a reduction of entropy when a chain is brought to the vicinity of the membrane. The associated free energy cost, of the order of a few k_BT [13], where k_B is the Boltzmann constant and T the absolute temperature, can thus cancel out the effective affinity between the phospholipid membrane and the cargo-bearing CPP.

Despite their affinity for zwitterionic membranes, CPPs like TAT are not able to penetrate the bilayers in the absence of a significant amount of charged lipid or phosphoethanolamine head groups[4]. This is consistent with the results of our experiments with TAT and Arg-functionalized ELP_{BC}, as we did not observe any permeability of the membranes by CPP-functionalized ELP_{BC}. In fact, the residual intensity inside the GUVs does not evolve over time and always exhibits negligible values even when the vesicles are exposed over 24 hours to the unimer ELP_{BC} solution (see Supplementary Table S2 and Supplementary Fig. S1).

Self assembly rescues the loss of affinity caused by cargo attachment. All of the diblock ELPs included in this study self-assemble into micelles when the solution is heated above their CMT, see Table 1. The non-functionalized ELP_{BC} at this temperature, despite its self-assembly into micelles, does not show any accumulation on the membrane, similar to the observations with unimers of functionalized and non-functionalized ELP_{BC}. We next examined the interactions of the micellar assemblies of CPP-functionalized ELP_{BC} with the zwitterionic membranes of DOPC, by evaluating radial intensity profiles of confocal images of GUVs exposed to ELP_{BC} solutions above their CMT.

TAT-functionalized ELP_{BC} self-assemble into micelles and accumulate at the membrane surface, as shown in Fig. 1B. Self-assembly is therefore able to offset cargo-induced reduction of affinity. Several reasons can be invoked to explain such an increase in affinity. Most notably, the micellar aggregate of p diblock copolymers has a much lower translational entropy than the corresponding p unimers. Therefore, attachment of one micelle implies loosing the entropy corresponding to one degree of freedom, while attachment of p unimers would imply loosing a much larger entropy corresponding to p degrees of freedom. This is similar to adsorption phenomena

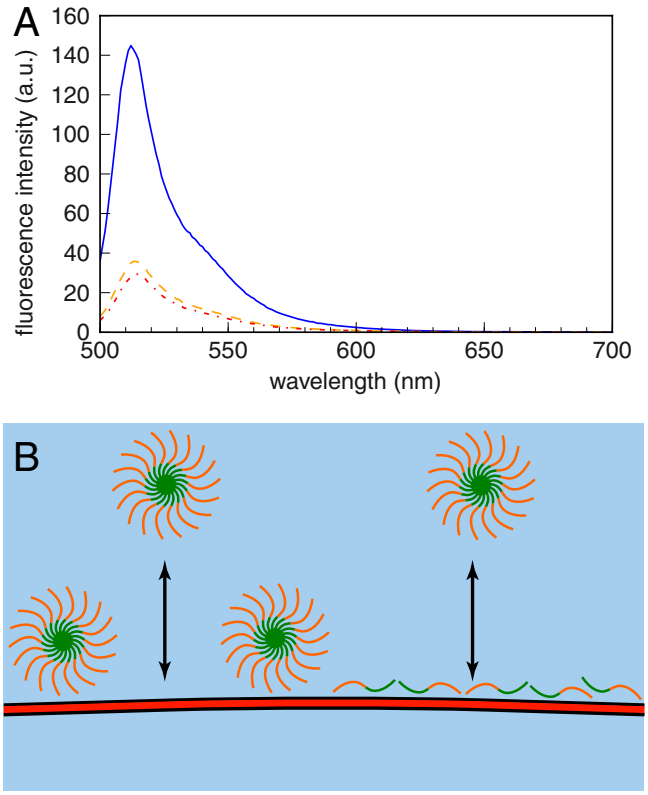

Figure 2. (**A**) Spectrum of a 50% BODIPY-labeled Arg_8–ELP_{BC} solution in the unimer state at 25 °C (blue solid line) recorded on a spectrofluorimeter. A reduction by self-quenching of around 75% is observed at 40 °C (orange dashed line) and 42 °C (red dashed dotted line). (**B**) Schematic illustration of two possible scenarios for ELP_{BC} adsorption on the phospholipid bilayer, either as micelles or in the unimer state. The arrows emphasize that the attachment process is ruled by the chemical equilibrium between the surface and the bulk[16].

of high molecular weight polymers that can adsorb strongly at interfaces even with modest (less than k_BT) energy of interaction per monomer[12]. Also, the self-assembly of diblock copolymers into a single micelle induces conformational changes in the hydrophilic block of the ELP_{BC}, leading to a distribution of the end-functional groups that is more favourable for interactions with a wall[14].

Arg_8-functionalized ELP_{BC} display behaviour similar to TAT-functionalized ELP_{BC}. Indeed, a quantitative analysis of the fluorescence intensity profiles, explained in the Methods below, revealed similar number coverages for both TAT- and Arg_8-functionalized ELP_{BC} with N_{PTL}, the number of polypeptides per thousand lipids, of the order of 10; more precisely we obtained $N_{PTL} = 13 \pm 3$ for TAT-ELP_{BC} and $N_{PTL} = 6 \pm 5$ for Arg_8–ELP_{BC}. Such values correspond to a surface mass coverage of ~1 mg m^{-2}, comparable to the values obtained for moderate strength adsorption of polymers on surfaces[12].

In contrast, Arg_5-functionalized ELP_{BC} show no accumulation on the membrane despite their micellar state in solution. Our results thus show that interactions with the membrane can be finely tuned by the arginine content of the CPP that is present at the extremity of the the hydrophilic block of the ELP_{BC}.

It is remarkable that despite the increase in affinity for the membrane, the self-assembled micelles of diblock polypeptides do not permeate across the bilayers. Similarly to the case of unimer solutions, the measured relative intensities inside the GUVs are consistently low, even for long periods of incubation (see Supplementary Table S2). The absence of equilibration between inner and outer fluorescence levels gives an upper bound of 10^{-4} μm s^{-1} for the permeability of DOPC bilayers with respect to ELP_{BC}, which is several orders of magnitude lower, for instance, than the permeability of DOPC to AF488 at 1.7 10^{-2} μm s^{-1} [15].

We qualitatively observed that the precise kinetics of attachment of ELP_{BC} to the membrane depends on the exact temperature in the observation chamber, but did not precisely study how faster attachment occurs with increased temperature. Despite such effects, attachment always leads to a polypeptide corona that can be detached from the membrane if the temperature is lowered below the CMT. This shows that the binding mechanisms in our case are a result of a chemical equilibrium between the adsorbed layer and the solution.

Micellar vs. unimer adsorption on the membrane. Polypeptide coverage amounts on the order of 1 mg m^{-2} can be rationalized equally by the attachment of micelles or unimer polypeptides to the membrane, as displayed in Fig. 2B. In order to discriminate between these two possible scenarios, we incorporated BODIPY–a fluorophore that self-quenches significantly at high local concentration–into the ELP_{BC} as shown in Fig. 2A. Indeed, a significant reduction of fluorescence intensity is observed in solution upon assembly into micelles for

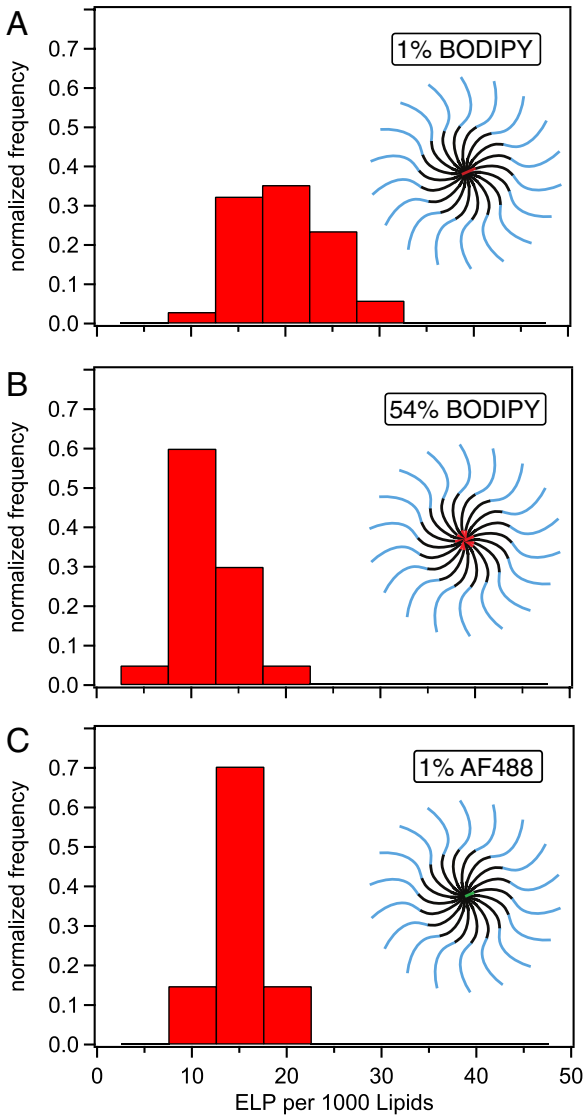

Figure 3. Distribution of N_{PTL} values for samples containing different mixtures of labelled and unlabelled TAT-ELP_{BC}. (**A**) with 1% of BODIPY-labeled TAT-ELP_{BC} (**B**) with 54% of BODIPY-labeled TAT-ELP_{BC} and (**C**) with 1% of AF488-labeled TAT-ELP_{BC}. Histograms of normalized frequency (the values of the histogram bars add up to one) in (**A**–**C**) were computed from respectively 34, 40 and 27 vesicle profiles. Experiments were performed at 35 °C.

samples containing 54% BODIPY-labeled ELP_{BC}. Note that for samples with fractions of BODIPY-labeled ELP_{BC} below 10%, no quenching is observed.

We performed and analyzed experiments under conditions similar to those described above for the AF488. Three different types of ELP_{BC} solutions were prepared: (A) TAT- ELP_{BC} with 1% of BODIPY-labeled TAT-ELP_{BC}, (B) TAT-ELP_{BC} with 54% of BODIPY-labeled TAT-ELP_{BC} and (C) TAT-ELP_{BC} with 1% of AF488-labeled TAT-ELP_{BC}. Figure 3 shows histograms for the values of surface peptide coverage expressed as N_{PTL}, the number of peptides per 1000 lipids–calculation described in the Methods section–obtained for the three types of samples described above. The average number of adsorbed ELP_{BC} per 1000 lipids does not display any significative difference between the three measurement conditions, with an average close to 13 ± 5, corresponding to a mass coverage of $\sim 1.4 \pm 0.5\,mg\,m^{-2}$.

Comparison between the first two histograms in Fig. 3 shows that TAT-functionalized ELP_{BC} adsorb in their micellar form. Indeed, if breakage of the micelles occurred, samples with 54% BODIPY-labeled ELP_{BC} ($N_{PTL} = 9 \pm 3$) should display significantly larger apparent values for N_{PTL} than the sample with 1% of BODIPY-labeled TAT-ELP_{BC} ($N_{PTL} = 17 \pm 5$) due to dequenching at the membrane surface. Note also that samples with 1% of AF488-labeled TAT-ELP_{BC} ($N_{PTL} = 13 \pm 2$) and samples with 1% of BODIPY-labeled TAT-ELP_{BC} ($N_{PTL} = 17 \pm 5$) give comparable results showing that the method is independent of the flurophore.

It is interesting to note that at the polypeptide bulk concentrations (20 μM) where our experiments were performed the surface is not completely saturated with micelles. Indeed, the measured adsorption of micelles

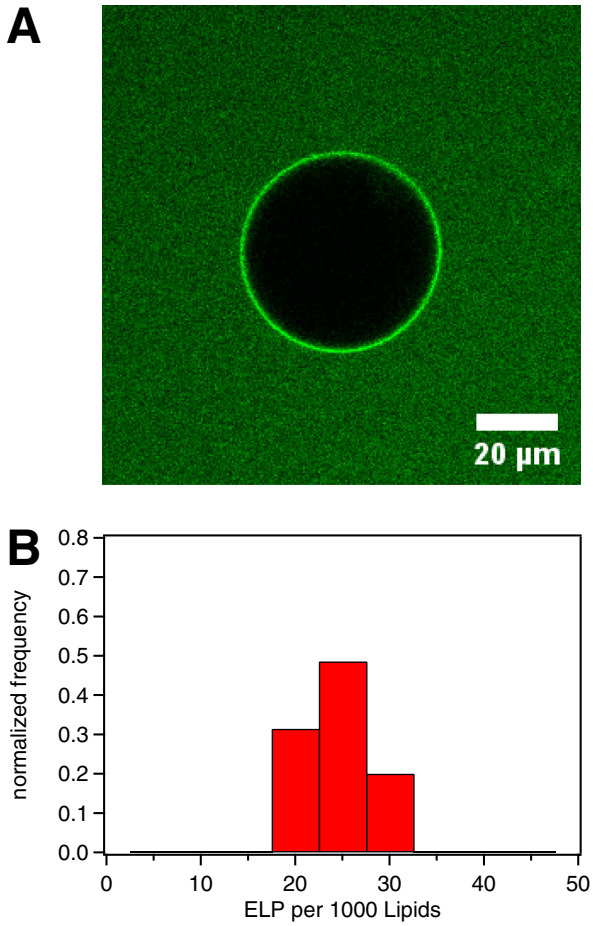

Figure 4. (**A**) Typical image from confocal microscopy of a GUV from a ternary mixture of DOPC/DOPE/DOPG at molar fractions of 65/25/10 exposed to a TAT-functionalized ELP_{BC} above its micellization temperature. (**B**) The corresponding histogram of measured N_{PTL} values from 35 GUVs. Here all experiments were performed at 35 °C.

corresponds to about half of full coverage (43% ± 16% of occupied projected area) of the membrane surface by micelles, as calculated from an aggregation number of 89 and a radius of 25.9 nm for the TAT-ELP_{BC} micelle. For comparison, if one would cover the surface with a triangular network of a dense packing of monodisperse hard spheres, a coverage of ~90% would be reached.

DOPC/DOPE/DOPG vesicles. It has been shown that zwitterionic bilayers enriched with anionic lipids promote the adsorption of TAT without any attached cargo on the lipid membrane, but only lead to vesicle penetration when molar fractions of charged lipids reached values much larger than those that are biologically relevant[4]. Penetration is, however, observed when membranes are prepared from mixtures of DOPC and DOPE, a lipid promoting negative leaflet curvature. We prepared GUVs from the ternary lipid mixture DOPC/DOPE/DOPG at molar fractions of 65/25/10, comparable to the typical phospholipid head composition of mammalian cells. For these systems, we observed a behaviour similar to that of TAT-functionalized ELP_{BC} interacting with zwitterionic membranes. At room temperature, exposure of the GUVs to the solution of the TAT-ELP_{BC} in the unimer form did not lead to the accumulation of peptide on the lipid bilayer, despite of the presence of the negative charges associated with the DOPG, thus confirming a very significant reduction of the CPP affinity to the membrane due to the ELP_{BC} cargo. At temperatures above micellation, an accumulation corona similar to that observed for the zwitterionic membranes also built up, albeit with faster kinetics, typically on the order of ten minutes, and with larger peptide coverage values, $N_{PTL} = 22 \pm 3$, see Fig. 4. Also, similarly to zwitterionic membranes, no translocation of micelles across the ternary membrane was observed, thus further supporting that in cells the observed uptake of ELP_{BC} micelles occurs by active pathways such as endocytosis.

Discussion

By performing experiments with GUVs composed of the zwitterionic lipid DOPC, we monitored the interactions between the lipid bilayer and a class of cargo-bearing CPPs by fluorescence confocal laser scanning microscopy. Although cationic CPPs display an affinity for bilayers of phosphorylcholine lipids, the attachment of a polymeric cargo like ELP_{BC} suppresses membrane binding interactions. This suppression was also observed for the TAT-functionalized ELP_{BC} with the anionic ternary lipid mixture DOPC/DOPE/DOPG with composition

65/25/10, showing that cargo-induced suppression of binding interactions occurs even with membranes bearing 10% anionic lipid heads.

We have shown that binding to the membrane can be recovered by cargo self-assembly into micelles. The resulting structures, which can be simply pictured as soft nanospheres decorated by CPP sequences, adsorb onto the membrane in their micellar form. However, recovery of affinity depends critically on the number of arginine units in the CPP sequence and it requires more than five arginine residues for this system. Significantly, no penetration was observed either for the unimer or the micellar forms independent of their arginine content. These results on DOPC membranes were also confirmed for the interactions between TAT-functionalized ELP_{BC} and ternary lipid mixtures mimicking mammalian cell compositions. Crucially, this sheds light on previous results, wherein it was shown that self-assembly of CPP-functionalized ELP_{BC} increased cellular uptake for several cell lines[9,11]. Our results suggest that uptake is controlled by a first step where self-assembled micelles passively bind to the plasma membrane, before they are actively internalized by cellular mechanisms. The increased uptake of ELP_{BC} micelles bearing Arg_8 and TAT on their corona is simply due to the increase of interfacial concentration of the micelles at the cell membrane in contrast to the same cargo in its unassembled unimer state.

Our work paves the way not only for designing a strategy for the rational design of CPP based intracellular delivery systems, but provides also a platform for comparing delivery efficiency of CPP based systems with conceptually similar vehicles such as those provided by lipid nanoparticles[17,18].

Methods

Materials. Phospholipids used in this work are 1,2-dioleoyl-sn-glycero-3-phosphocholine (DOPC), 1,2-dioleoyl-sn-glycero-3-phosphoethanolamine (DOPE) and 1,2-dioleoyl-sn-glycero-3-phospho-(1′-rac-glycerol) (DOPG) (99%, Avanti-lipids, Alabaster, Al). Lipids were purchased in powder form, dissolved in chloroform and stored at −20 °C before use. Chloroform, sucrose, glucose and phosphate-buffered saline tablets (PBS, 0.01 M phosphate buffer, 0.0027 M KCl and 0.137 M NaCl, pH 7.4) were purchased from Sigma Aldrich as analytical grade chemicals. All of the chemicals were used without further purification.

Synthesis of functionalized ELP_{BC}. ELP_{BC} were named by their CPP-functionalization of the C-terminal of the ELP_{BC}: Arg_5–ELP_{BC}, Arg_8–ELP_{BC}, TAT-ELP_{BC} (47YGRKKRRQRRR57) and a ELP_{BC} non-functionalized control. Arg_5–ELP_{BC} and its respective non-functionalized control ELP_{BC} were genetically designed by Recursive Directional Ligation (RDL) as described elsewhere[19]. Arg_8–ELP_{BC}, TAT-ELP_{BC} and their respective control ELP_{BC} were genetically designed by RDL by plasmid reconstruction (PRe-RDL)[20]. All of the ELP_{BC} possess a 'leader' sequence (GCGWPG), the Arg_5–ELP_{BC} was composed by the following peptide sequence $(VPGVG)_{60}$ -$(VPGXG)_{[X=V:G:A,1:7:8]_{96}}$ and the rest of the ELP_{BC} by $(VPGVG)_{60}$ -$(VPGAGVPGGG)_{30}$.

E. coli containing the ELP genes were grown 24 hours at 37 °C while shaking in the presence of ampicillin or kanamycin. *E. coli* were collected by centrifugation and cells were lysed by sonication. ELP_{BC} were purified by their thermal properties by inverse transition cycling[21]. For fluorescent labeling AF488 C5-maleimide or BODIPY FL-maleimide was conjugated to a cysteine residue on the N-terminus of the ELP_{BC} in the presence of 3 mM TCEP-HCl and 10 mM NaH_2PO_4 at a pH of 7 for 2 hours. Aggregation of ELP_{BC} was induced by addition of NaCl, the labeled ELP_{BC} was collected by centrifugation and the supernatant was discarded. Afterwards the ELP_{BC} were resuspended in PBS buffer solution and remaining free fluorophore was removed with a desalting column. Dialysis was performed against water and the ELP_{BC} were lyophilized. The lyophilized ELP_{BC} were stored at −20 °C and resuspended in PBS solution at a concentration between 16–25 μM before use.

The temperature dependent self-assembly of ELP_{BC} at 25 μM in PBS buffer was monitored with dynamic light scattering (DLS) in the range between 25 °C and 50 °C. The critical micellar temperature and the hydrodynamic radius were determined, see Table 1. The aggregation number was determined by static light scattering (SLS) at 37 °C. Supplementary Fig. S2 shows an example of a recorded temperature dependent DLS. Values of the CMT and the hydrodynamic radius of the micelles are insensitive to conjugation of fluorophore.

Preparation of GUVs. GUVs were prepared by following the electroformation method of Angelova *et al.*[22]. Briefly, 10 μL of the lipid solution (1 mg ml^{-1} in chloroform) were spread on an indium tin oxide (ITO) coated glass slide. After drying the lipid film under vacuum for 30 min, a chamber was formed with a second ITO slide and Sigillum wax (Vitrex, Copenhagen, Denmark) as sealing agent. This chamber was filled with sucrose solution. The osmolarity of the solutions was measured with an osmometer (Osmomat 030, Gonotec, Berlin, Germany) and adjusted to 280 mOsm kg^{-1}. An alternating electric field was applied across the chamber for 3–12 hours at room temperature. The amplitude and the frequency of the field were set to 1 V and 10 Hz. Successful formation was checked by observing the growing chamber by phase contrast microscopy. The obtained GUVs were transferred to an Eppendorf tube, diluted one time with isoosmotic PBS or glucose solution and left undisturbed for 15 min before further use.

Interactions of ELP_{BC} with GUVs. The ELP_{BC} were dissolved in a 280 mOsm kg^{-1} PBS solution in a concentration range of 16 to 25 μM. The solutions were adjusted such that around 0.5% of the ELP_{BC} were fluorescently labeled with AF488. For a typical experiment three volume parts of the solution containing the ELP_{BC} were mixed with one volume of the previous prepared vesicle solution. Parallel samples were usually prepared and incubated at 25 °C (below CMT) and at 35 °C (above CMT). Samples were incubated for 1.5–2 hours directly under the confocal microscope, using a home made heating cell (Supplementary Fig. S3). Out of focus light was minimized by imaging the GUV at the equator of the vesicle.

The observation directly under the microscope allowed additionally the measurement of the partition coefficient of a single GUV as a function of time. After incubation, image recording of random GUVs within the sample was started and usually finished after a maximum of two hours for the whole experiment.

Optical microscopy. Vesicle contours were imaged by phase contrast microscopy or differential interference contrast microscopy (DIC) using an inverted TE 2000 microscope (Nikon, Japan) equipped with a 60x WI/1.2NA Plan Apo DIC objective or 40x Ph2/NA 0.60 Plan Fluor objective. Images were recorded with a digital camera (Hamamatsu EM-CCD, Japan) with a pixel depth of sixteen bits. The reflection interference contrast microscopy technique (RICM) was used with a 100x NA 1.4 Plan Apo objective for locating adhered vesicles (Supplementary Fig. S5).

Fluorescent imaging was performed using confocal laser scanning microscopy (CLSM) with a Nikon C1 scanhead. Images were captured using EZ-C1 software (Nikon, version 3.50). The AF488 and BODIPY labeled ELP_{BC} were excited using a argon-ion laser (Melles-Griot) at 488 nm.

Quantitative measurements of adsorbed amount from image analysis. Quantitative analysis of fluorescent intensities in the confocal images was performed using radial, angularly averaged, intensity profiles extracted with the "radial profile extended plugin" from Philippe Carl from the ImageJ homepage. To ensure that the measured fluorescence intensity of the fluorescently labeled ELP_{BC} behaves linearly with the concentration of the fluorophores, a fluorescence intensity curve was recorded with the confocal microscope at different heights from the glass slides (Supplementary Fig. S4). Furthermore, in order to properly account for possibly different acquisition parameters for different experiments, a calibration method (Supplementary Methods) was developed. For quantification of the adsorbed ELP_{BC} amount, the excess fluorescence above the level of sigmoidal profile for non decorated membranes was evaluated and Γ, the number of ELP_{BC} per unit membrane surface was extracted from

$$\Gamma = \frac{c_b}{R}\int_0^\infty r\,dr\,\frac{I(r) - I_0(r)}{I_b} \tag{1}$$

where $I(r)$ is the radial profile intensity in the presence of excess coronal intensity, $I_0(r)$ the intensity profile in absence of corona, $I_b = I(r \to \infty) = I_0(r \to \infty)$ the bulk intensity, c_b the bulk number concentration of the ELP_{BC} and R the radius of the vesicle. Equation 1 assumes equal quantum yields for fluorophores in the bulk and in the vicinity of the membrane, a valid assumption for fluorophores which do not penetrate the membrane, at fluorophore surface concentrations below self-quenching values. For our particular case we convert Γ to the more informative quantity N_{PTL}, the number of polypeptides adsorbed per thousand lipids by using

$$N_{PTL} = 1000\,\Gamma\,A_L \tag{2}$$

with A_L the area of a lipid. Given that for DOPC $A_L \simeq 0.7\,nm^2$, N_{PTL} represents here the number of peptides in a lipid patch of roughly 25×25 square nanometers.

References

1. Madani, F., Lindberg, S., Langel, U., Futaki, S. & Gräslund, A. Mechanisms of cellular uptake of cell-penetrating peptides. *J Biophys* **2011,** 414729 (2011).
2. Schmidt, N., Mishra, A., Lai, G. H. & Wong, G. C. L. Arginine-rich cell-penetrating peptides. *FEBS Lett* **584,** 1806–13 (2010).
3. Koren, E. & Torchilin, V. P. Cell-penetrating peptides: breaking through to the other side. *Trends in molecular medicine* **18,** 385–393 (2012).
4. Ciobanasu, C., Siebrasse, J. P. & Kubitscheck, U. Cell-penetrating HIV1 TAT peptides can generate pores in model membranes. *Biophysical journal* **99,** 153–162 (2010).
5. Thorén, P. E. *et al.* Membrane binding and translocation of cell-penetrating peptides. *Biochemistry* **43,** 3471–3489 (2004).
6. Tünnemann, G. *et al.* Cargo-dependent mode of uptake and bioavailability of TAT-containing proteins and peptides in living cells. *The FASEB journal* **20,** 1775–1784 (2006).
7. Vasconcelos, L. *et al.* Effects of cargo molecules on membrane perturbation caused by transportan10 based cell-penetrating peptides. *Biochimica et Biophysica Acta (BBA)-Biomembranes* **1838,** 3118–3129 (2014).
8. Maiolo, J. R., Ferrer, M. & Ottinger, E. A. Effects of cargo molecules on the cellular uptake of arginine-rich cell-penetrating peptides. *Biochim Biophys Acta* **1712,** 161–72 (2005).
9. MacEwan, S. R. & Chilkoti, A. Digital switching of local arginine density in a genetically encoded self-assembled polypeptide nanoparticle controls cellular uptake. *Nano Lett.* **12,** 3322–8 (2012).
10. Dreher, M. R. *et al.* Temperature triggered self-assembly of polypeptides into multivalent spherical micelles. *J. Am. Chem. Soc.* **130,** 687–694 (2008).
11. MacEwan, S. R. & Chilkoti, A. Controlled apoptosis by a thermally toggled nanoscale amplifier of cellular uptake. *Nano Lett* **14,** 2058–64 (2014).
12. Fleer, G., Stuart, C. & Scheutjens, J. *Polymers at interfaces* (Springer, 1993).
13. DeGennes, P. G. *Scaling concepts in polymer physics* (Cornell University Press, 1979).
14. Johner, A. & Joanny, J. F. Adsorption of polymeric brushes: Bridging. *The Journal of chemical physics* **96,** 6257 (1992).
15. Nishimura, K. *et al.* Identification of giant unilamellar vesicles with permeability to small charged molecules. *RSC Advances* **4,** 35224–35232 (2014).
16. Johner, A. & Joanny, J. Block copolymer adsorption in a selective solvent: a kinetic study. *Macromolecules* **23,** 5299–5311 (1990).
17. Rädler, J. O., Koltover, I., Salditt, T. & Safinya, C. R. Structure of DNA-cationic liposome complexes: DNA intercalation in multilamellar membranes in distinct interhelical packing regimes. *Science* **275,** 810–4 (1997).
18. Dias, R. S. *et al.* Interaction between DNA and cationic surfactants: effect of DNA conformation and surfactant headgroup. *J Phys Chem B* **112,** 14446–52 (2008).
19. Meyer, D. E. & Chilkoti, A. Genetically encoded synthesis of protein-based polymers with precisely specified molecular weight and sequence by recursive directional ligation: examples from the elastin-like polypeptide system. *Biomacromolecules* **3,** 357–367 (2002).
20. McDaniel, J. R., Mackay, J. A., Quiroz, F. G. & Chilkoti, A. Recursive directional ligation by plasmid reconstruction allows rapid and seamless cloning of oligomeric genes. *Biomacromolecules* **11,** 944–52 (2010).

21. Meyer, D. E. & Chilkoti, A. Purification of recombinant proteins by fusion with thermally-responsive polypeptides. *Nat. Biotechnol.* **17,** 1112–1115 (1999).
22. Angelova, M. I. & Dimitrov, D. S. Liposome electroformation. *Faraday Discuss.* **81,** 303–311 (1986).

Acknowledgements
A.W. and C.M. thank the IRTG Soft Matter Science and the Région Alsace for funding, A.C acknowledges the NIH for support of this research through grant NIH R01EB007205, and S.M. and A.C. acknowledge the support of this research by the Research Triangle MRSEC through grant NSF DMR-1121107. C.M. is thankful for support from CNPq under PVE 400997/2014-2 and from FAPESP under visiting professor project 2015/07508-5.

Author Contributions
S.M. synthesized and characterized ELPs. A.W., V.W., P.M., A.S. and T.S. performed and interpreted measurements on GUVS in ELP solutions. C.M. and A.C. designed and supervised the project. C.M., A.W. and V.W. wrote the paper. All authors provided feedback on the manuscript.

Additional Information
Supplementary information accompanies this paper at http://www.nature.com/srep

Competing Interests: The authors declare no competing financial interests.

How to cite this article: Weinberger, A. *et al.* Cargo self-assembly rescues affinity of cell-penetrating peptides to lipid membranes. *Sci. Rep.* **7**, 43963; doi: 10.1038/srep43963 (2017).

Publisher's note: Springer Nature remains neutral with regard to jurisdictional claims in published maps and institutional affiliations.

Supplementary Information for: Cargo self-assembly rescues affinity of cell-penetrating peptides to lipid membranes

Andreas Weinberger[1,+], Vivien Walter[1,+], Sarah R. MacEwan[2,3], Tatiana Schmatko[1], Pierre Muller[1], André P. Schröder[1], Ashutosh Chilkoti[2], and Carlos M. Marques[1,*]

[1]Université de Strasbourg, CNRS, ICS UPR 22, F-67000 Strasbourg, France
[2]Duke University, Department of Biomedical Engineering, Durham, North Carolina, United States
[3]Current address: University of Chicago, Institute for Molecular Engineering, Chicago, Illinois, United States
[*]marques@unistra.fr
[+]these authors contributed equally to this work

Supplementary Tables

Table S1. Acronyms used in this paper

AF488	Alexa Fluor 488
Arg_x	Oligoarginine with x arginines
BODIPY	Boron-Dipyrromethene
CMT	Critical Micellization Temperature
CPP	Cell Penetrating Peptide
DIC	Differential Interference Contrast
DOPC	1,2-dioleoyl-sn-glycero-3-phosphocholine
DOPE	1,2-dioleoyl-sn-glycero-3-phosphoethanolamine
DOPG	1,2-dioleoyl-sn-glycero-3-phospho-(1'-rac-glycerol)
ELP	Elastin-like Polypeptide
ELP_{BC}	Elastin-like Polypeptide block copolymer
GUV	Giant Unilamellar Vesicle
N_{PTL}	Number of Polypeptides adsorbed per Thousand Lipids
RICM	Reflexion Interference Contrast Microscopy
PM	Photomultiplier
TAT	Trans-Activator of Transcription

Table S2 summarizes the relative intensities inside the vesicles obtained for incubation with functionalized ELP_{BC} above and below the CMT of the ELP_{BC}. The non-vanishing values are likely to be related both to the mixing process during sample preparation and to light pollution from the glass surfaces when the GUVs are strongly adsorbed, see Figure S5. By tracking a single vesicle during an incubation time of 1 hour after mixing, it could be shown that the internal intensity does not increase with incubation time (Figure S1). Longer incubation time of up to 24 hours did not lead to any further increase of the internal intensity. For experiments performed with ELP_{BC} in their micellar state above the CMT an increased dispersion of the values and a higher initial intensity value could be observed. The higher initial values are likely to be determined during mixing.

Table S2. Relative GUV internal intensity in % for different types of ELP_{BC} incubated with GUVs of DOPC at 25 °C and above CMT. Relative intensity values do not correlate with incubation times that range here from 2 to 24 hours.

ELP-Type	Fluorophore	25 °C		above CMT	
		Mean	SD	Mean	SD
Arg_5	AF488	7.12	2.79	8.86	4.26
Arg_8		9.00	2.16	16.22	8.59
TAT		8.18	1.33	20.53	13.33
No function		5.79	2.37	8.26	3.34
Arg_8	BODIPY	6.93	1.52	19.42	9.89
No function				21.07	5.9

Supplementary Figures

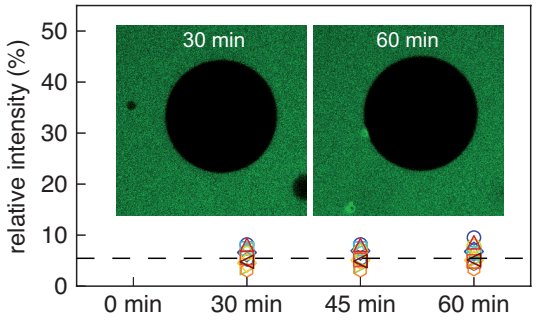

Figure S1. No change of relative internal fluorescence intensities within one hour. After 30 min of stabilization, recording was started. The confocal pictures show one DOPC vesicle surrounded by a PBS Buffer solution containing Arg_5-functionalized ELP_{BC} at 40 °C, similar results are obtained with other functionalizations. No change in relative intensities can be observed. Each symbol stands for one single GUV per sample. Different symbols signify different functionalities and incubation temperatures. Vesicle diameter is 35 μm.

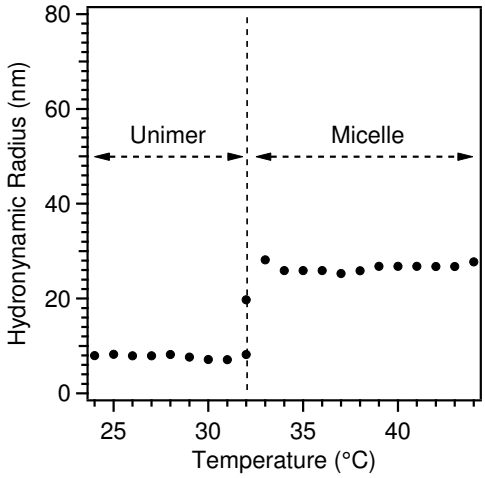

Figure S2. ELP_{BC} form micelles above the CMT as shown by measurement of the hydrodynamic radius by DLS. Soluble unimers of TAT-ELP_{BC} existed with a R_h below 10 nm up to 32 °C. At 32 °C self-assembly into micelles occurred. Micelles with a R_h of approximately 30 nm were formed. At temperatures above 50 °C micrometer size aggregates were formed. Measurements at 25 °C and 37 °C were repeated five times, with measured deviations of about 2%.

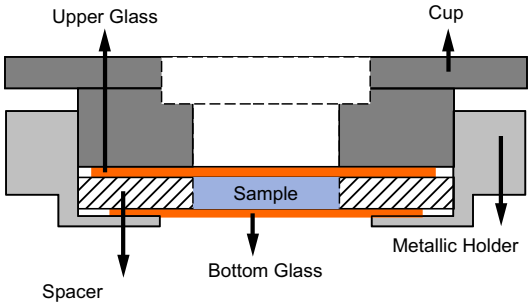

Figure S3. Home-made heating cell for observations and incubation directly under the microscope. The objective under the cell is also temperature-regulated. Due to heat loss, the temperature of the heating bath that warms the metallic holders had to be adjusted for different experiments, to ensure appropriate temperatures in the chamber within the micellar range of the ELP_{BC}.

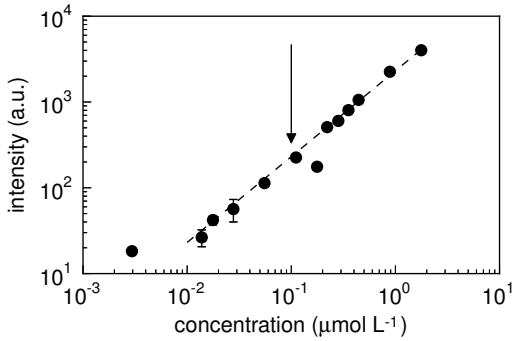

Figure S4. Fluorescence calibration curve for a solution of a control ELP_{BC} labeled with AF488 at room temperature, with the intensity given as a function of fluorophore concentration. The arrow represents the typical working conditions. The values were measured at 20 μm, 50 μm, 80 μm and 130 μm from the glass surface. Points represent the mean value of the four different positions and errorbars the standard deviation.

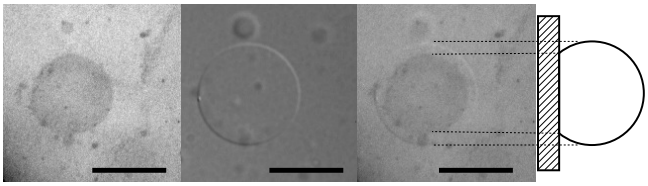

Figure S5. RICM (left) and DIC (center) images of GUVs incubated in TAT and Arg_8 functionalized ELP_{BC} solution above the CMT. Additionally to the appearance of the corona (as described in the main text), GUVs started to adhere on the glass surface of the heating cell, as observed by RICM, indicating attractive interactions between the CPP residues, the membrane and the glass surface. The right image superimposes the RICM and the DIC images. Scale bars 20 μm.

Supplementary Methods: calibration of the confocal images

The proportionality between the local sample concentration of fluorophores and the intensity displayed in the confocal image is a key requirement to extract the adsorbed fluorophore amount per unit surface of the membrane, a quantity in our work better expressed as the number of polypeptides adsorbed per thousand lipids or N_{PTL}. It is easy to realise however that analysis of images collected from the same vesicle for different acquisition parameters, such as the photomultiplier gain or the laser power might not yield the same N_{PTL} values even after the trivial expected corrections, see Fig. S6. Here, we present a method to easily account for these variations and assure the extraction of proper N_{PTL} values from the images.

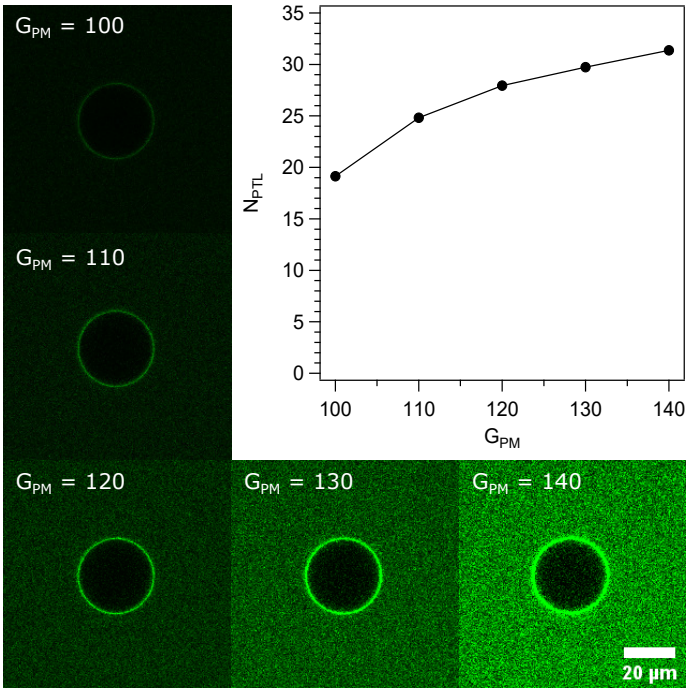

Figure S6. N_{PTL} measured from the raw intensity radial profile of the same vesicle, taken with different photomultiplier gains. Pictures display the PM gain G_{PM} used for acquisition, ranging from 100 to 140. The objective of the calibration procedure is to ensure stable measurement of N_{PTL} for all practical acquisition conditions.

The settings of the confocal microscope

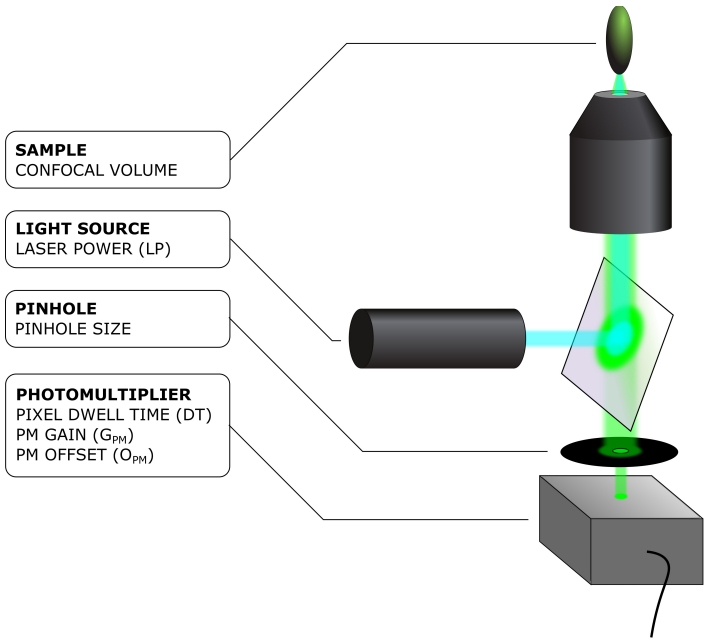

Figure S7. Simplified representation of the elements of the confocal microscope, highlighting the different parameters and settings which have an impact on the measured fluorescence intensity. All experiments are performed with the same objective at a fixed pinhole size.

The different parameters controlling the intensity value $I_P(x,y)$ acquired for each image pixel at the point (x,y) are shown in Fig. S7. Although the photomultiplier (PM) responds linearly to the number of collected photons, albeit with an offset O_{PM},

several spurious factors such as electronic noise contribute also to a background of the signal and need to be accounted for. In general the recorded pixel intensity value I_P is thus related to the relevant intensity I through

$$I_P(x,y) = A(G_{PM},DT)I(x,y) + B(O_{PM},DT) \tag{S1}$$

where $A(G_{PM},DT)$ is a prefactor that depends on the PM gain G_{PM} and on the dwell time DT. The background factor $B(O_{PM},DT)$ depends on the PM offset O_{PM} and on DT. The laser power LP changes also the pixel value I_P because the sought intensity I is proportional to LP, which of course does not perturb the calculation of N_{PTL}. Consistently we also found that the factors A and B in equation S1 do not depend on LP.

Calibration

The calibration procedure amounts to determine the factors $A(G_{PM},DT)$ and $B(O_{PM},DT)$ of supplementary equation S1. The first part of the calibration was done with a reference non-fluorescent sample (a standard buffer without fluorophores), so that in equation S1 one has $I_P = B(O_{PM},DT)$. By measuring pixel values I_P while changing the settings of the microscope allows not only to extract the function $B(O_{PM},DT)$ – see figure S8 – but also to confirm that the background value does not depend on laser power, PM gain or even on pinhole size.

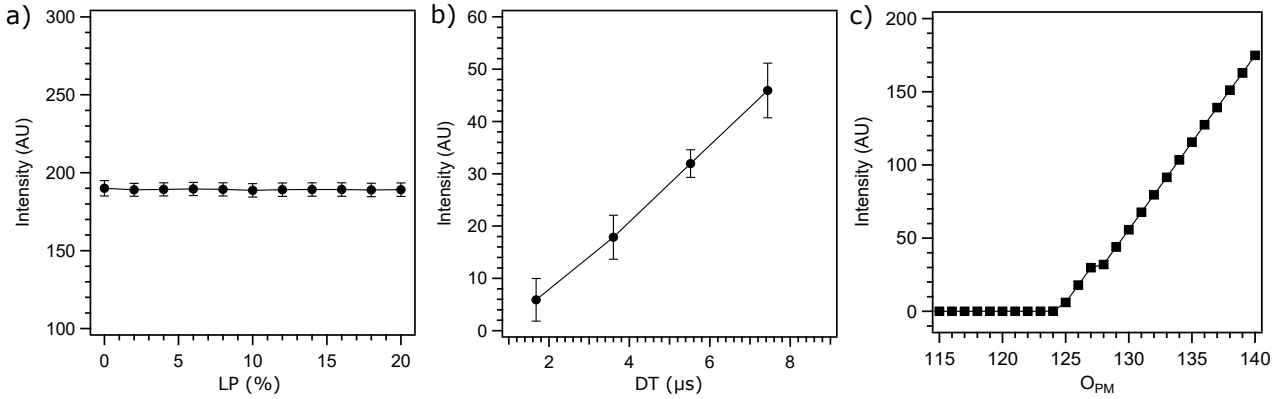

Figure S8. Calibration with a reference non-fluorescent sample, to determine the factor $B(O_{PM},DT)$ of equation S1. a) The measured intensity I_P is independent of the Laser Power LP. Intensity acquired with O_{PM}=150 and DT=3.6 μs; b) Variation of I_P with the Dwell Time DT. Here O_{PM}=128; c) The importance of the PM offset parameter O_{PM}. Here DT=5.52 μs.

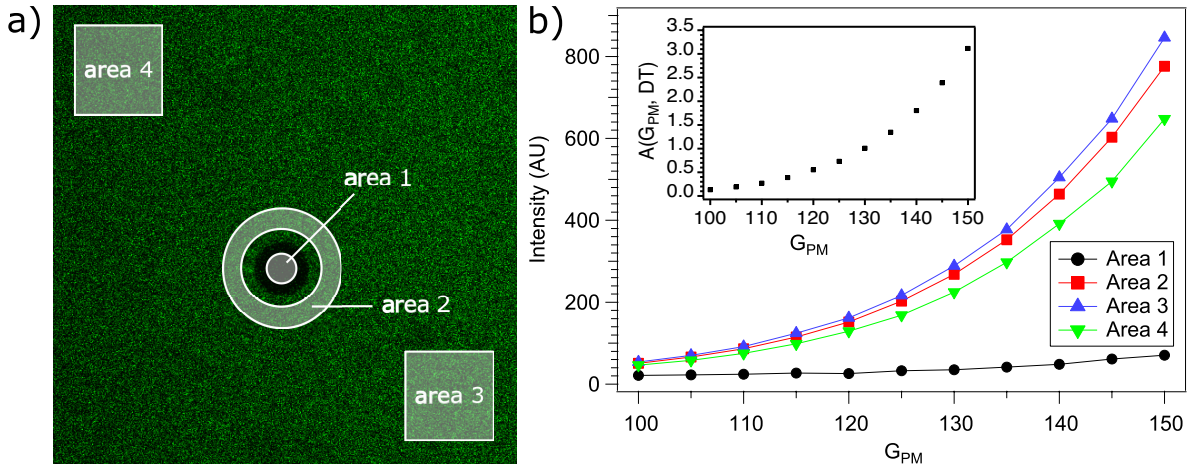

Figure S9. Calibration with a fluorescent sample containing non-fluorescent GUVs, to determine the factor $A(G_{PM},DT)$ of equation S1. a) The four zones of an image under analysis. b) Intensities of the four zones for different photomultiplier gains G_{PM} at constant DT=5.52 μs and O_{PM}=128. The factor $A(G_{PM},DT)$ obtained from the calibration is shown in the inset.

The second part of the calibration consists in extracting the factor $A(G_{PM},DT)$ by analysing the pixel values I_P of a number of different spots (four in our case) of images from a fluorescent solution containing non-fluorescent GUVs while changing

the value of the different acquisition parameters, see figure S9 for an example where the PM gain is changed at constant DT=5.52 μs and O_{PM}=128. Images from this system, where intensities vary due both to inhomogeneous light and fluorophore distributions, conveniently provides for images with a range of intensities and thus allows for acquiring different intensity values with the same image. The calibration consists of using supplementary equation S1 to find the function $A(G_{PM}, DT)$ that best gives identical "true" I values at the four points from the sample. The inset in figure S9 shows the obtained factor $A(G_{PM}, DT)$ for our particular case.

Checking the calibration

After calibration, supplementary equation S1 can be routinely used to extract the relevant values of sought intensity I. Also, one can check that derived quantities such as the intensity radial profiles normalized by the intensity of the bulk are independent of the acquisition parameters. An example of such a check is displayed in supplementary Fig. S10 for two different PM gains.

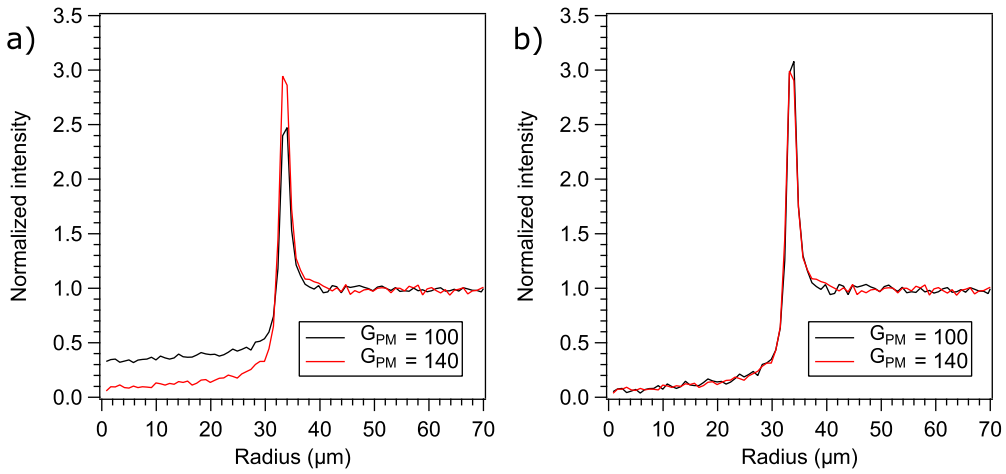

Figure S10. Intensity radial profiles acquired for two different PM gains and normalised with respect to the intensity of the bulk. (a) Raw values of the intensity. (b) Intensities after correction by the calibration equation S1.

Most importantly, the derived quantity N_{PTL} which is of relevance for our study, can now be computed independently of the acquisition parameters. As an example, we compare in supplementary figure S11 the values corresponding to the supplementary figure S6 before and after the calibration procedure.

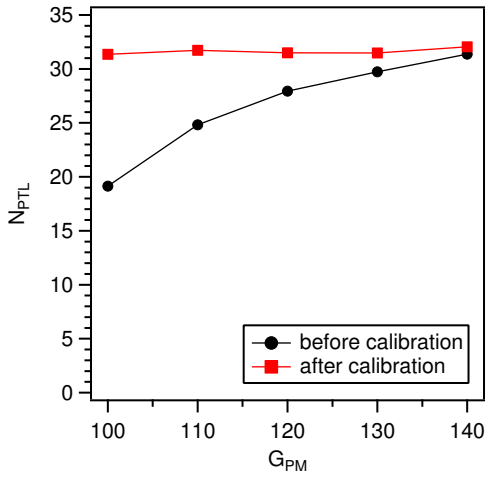

Figure S11. Comparison of the N_{PTL} values corresponding to images in figure S6, before and after the calibration procedure.